

Anomalous Hall effect in the noncollinear antiferromagnet Mn_5Si_3

Christoph Sürgers,^{1, a)} Wolfram Kittler,¹ Thomas Wolf,² and Hilbert v. Löhneysen^{1,2}

¹⁾Physikalisches Institut, Karlsruhe Institute of Technology, P.O. Box 6980, 76049 Karlsruhe, Germany

²⁾Institut für Festkörperphysik, Karlsruhe Institute of Technology, P.O. Box 3640, 76021 Karlsruhe, Germany

(Dated: 3 May 2018)

Metallic antiferromagnets with noncollinear orientation of magnetic moments provide a playground for investigating spin-dependent transport properties by analysis of the anomalous Hall effect. The intermetallic compound Mn_5Si_3 is an itinerant antiferromagnet with collinear and noncollinear magnetic structures due to Mn atoms on two inequivalent lattice sites. Here, magnetotransport measurements on polycrystalline thin films and a single crystal are reported. In all samples, an additional contribution to the anomalous Hall effect attributed to the noncollinear arrangement of magnetic moments is observed. Furthermore, an additional magnetic phase between the noncollinear and collinear regimes above a metamagnetic transition is resolved in the single crystal by the anomalous Hall effect.

I. INTRODUCTION

Today's spintronic devices mostly utilize the spin-dependent electronic transport in or between ferromagnets. For a long time, antiferromagnetic materials with zero net magnetization have rarely been considered to be of interest for information storage due to the difficulty to externally manipulate or read-out the magnetization state. However, quite recently, antiferromagnetic metal spintronic devices have been proposed to show current-induced phenomena like in ferromagnets such as spin-transfer torque^{1,2}, spin pumping², and domain-wall motion³. This opens up new opportunities in creating functional devices based on antiferromagnets as active components⁴. In addition, zero stray fields, reduced switching currents, and ultrafast switching by light⁵ are further advantages specific to antiferromagnets.

In solid-state electronic transport, the Hall effect takes a unique position because it probes electronic states directly at the Fermi level and the normal part of the Hall effect provides for single-band metals a measure of the Fermi volume, i.e., the volume in momentum space enclosed by the Fermi surface. At the onset of magnetic order additional contributions come into play and the measured Hall resistivity $\rho_{xy} = V_y t / I_x$ (V_y : Hall voltage across the sample width, I_x : current along direction x , t : sample thickness) comprises, in addition to the ordinary term arising from the Lorentz force acting on the charge carriers, a contribution called extraordinary or anomalous Hall effect (AHE)

$$\rho_{xy} = R_0 B_z + \rho_{xy}^{\text{AHE}} \quad (1)$$

where $B_z = \mu_0[H_z + (1 - N_z)M_z]$, and H_z , M_z , and N_z are the magnetic field, magnetization, and demagnetization factor, respectively, along the z direction perpendicular to the xy plane. Equation 1 is valid for low magnetic

fields, where the cyclotron frequency ω_c is much smaller than the mean scattering rate τ^{-1} of charge carriers, corresponding to $R_0 B \ll \rho_{xx}$.

In long-range ordered ferromagnets, the AHE is a consequence of the broken time-reversal symmetry and spin-orbit coupling (SOC)⁶. The latter leads to different scattering directions for spin-up and spin-down charge carriers which, together with the spin imbalance, creates a charge accumulation at opposite edges of the sample and a transverse electric field, i.e., a Hall voltage. The AHE is thought to arise from an extrinsic part attributed to energy-dissipative scattering and a dissipationless intrinsic part arising from the Berry-phase curvature of the Bloch states in momentum space^{6,7}. The individual contributions to the measured Hall voltage depend on the amount of scattering. The Berry-phase concept provides a link between the electronic band structure and the magnitude of the AHE⁶. In ferromagnets, SOC gives rise to a fictitious local field corresponding to a Berry potential. The scattering-independent Berry-phase contribution is more important for the AHE than for any other electronic transport coefficient. Recent studies⁸ revealed a crossover from the extrinsic (skew-scattering) region to the intrinsic region with increasing resistivity ρ_{xx} . Scaling the AHE provides a connection between the magnetic and transport properties, enabling the universality class of the phase transition to be reliably determined from the AHE with a prospect of studying the role of dimension on the critical behavior⁹.

A. Hall effect in noncollinear magnetic structures

Early descriptions¹⁰ of the AHE in an antiferromagnet (AFM) with two collinear sublattices of magnetization \mathbf{M}_1 and \mathbf{M}_2 considered a Hall effect proportional to the antiferromagnetic vector $\mathbf{L} = \mathbf{M}_1 - \mathbf{M}_2$. More recently, the AHE has been investigated in various systems with nontrivial arrangements of the magnetic moments. In these instances, the AHE was explained by the accumulated Berry phase of the electron when mov-

^{a)}christoph.suergers@kit.edu

ing through the spatially varying magnetization along its path, even without SOC. The remaining contribution to the AHE arising from the magnetic structure and not from SOC has been often related to a topological Hall effect (THE). A THE due to the Berry phase in *momentum space* was observed in $\text{Pr}_2\text{Ir}_2\text{O}_7$ and $\text{Nd}_2\text{Mo}_2\text{O}_7$ with pyrochlore structure where the localized spins do not exhibit long-range magnetic order^{11,12}. In the highly correlated metal UCu_5 , a chirality-induced 'geometrical Hall effect' independent of SOC has been shown to occur due to antiferromagnetically-coupled localized $5f$ -electron spins¹³. In the helimagnets MnGe , MnSi , or FeGe hosting a skyrmion lattice, a THE is due to the winding of the spin texture and the Berry potential in *real space*¹⁴. In fact, in this case the THE is a hallmark of skyrmion formation and has been used to reveal depinning and motion of skyrmions¹⁵. Emergence of a large AHE has also been predicted on the surface of an Fe monolayer on $\text{Ir}(001)$ ¹⁶.

In contrast to ferromagnets where it is often assumed that the anomalous part of the AHE depends linearly on M , $\rho_{xy}^{AHE} = S_H \rho_{xx}^2 M$, a vanishing AHE is expected for an AFM with zero net magnetization. However, it has been shown that the intrinsic part of the AHE due to the Berry-phase curvature is not zero if certain symmetries are broken, for instance due to an applied magnetic field or SOC¹⁷. Although in a collinear AFM the total symmetry recovers and no AHE is generated, a nonzero AHE occurs in a noncollinear magnetic arrangement independent of the strength of SOC which can even be zero. The THE due to the strongly noncollinear magnetization texture should vanish when a collinear magnetic state is induced by a magnetic field $H > H_c$. Alternatively, the AHE of an AFM should strongly change when the spin structure changes from collinear to noncollinear in dependence of temperature¹⁷.

In this respect, hexagonal Mn_3Ge and cubic Mn_3Pt or Mn_3Ir have been proposed to show a large AHE due to the nontrivial spin structure^{17–19}. Furthermore, antiferromagnetic Mn_5Si_3 is an interesting metallic compound which does show collinear and noncollinear phases at different temperatures and can thus serve as model system to study the different contributions to the AHE. In fact, an extra contribution to the AHE caused by the noncollinear magnetic structure and attributed to a THE has been reported for Mn_5Si_3 films²⁰. Non-collinearity may also be stabilized in the isostructural ferromagnet Mn_5Ge_3 by uniaxial distortion²¹. Mn_5Ge_3 and $\text{Mn}_5\text{Ge}_3\text{C}_x$ ($x \approx 1$) have been proposed as ferromagnetic electrodes for spintronic applications due to their ability to grow epitaxially on Si and GaAs substrates^{22–26}. In all these Mn compounds the different magnetic structures originate from the sensitivity of the Mn moment on the local atomic environment, in particular the Mn-Mn distances which are found to be the major factor leading to different site-dependent Mn moments²⁷. Here, we report on measurements of the electrical resistivity and AHE of a Mn_5Si_3 single crystal and polycrys-

talline thin films. The latter show indications of a THE in the noncollinear phase which is absent in the collinear phase and for large magnetic fields. A similar behavior is found for the single crystal albeit with a hysteresis in the AHE. Moreover, the metamagnetic transition at high fields gives rise to a strong contribution to the AHE which is absent in the polycrystalline films. Comparison of the data allows to reveal the contributions from different magnetic phases to the Hall effect, such as a metamagnetic transition, and suggests an intermediate magnetic phase between the noncollinear and collinear phase in this compound.

B. Antiferromagnetic Mn_5Si_3

In the paramagnetic state, the hexagonal unit cell (space group $\text{P6}_3/\text{mcm}$) with lattice parameters a_h and c_h contains Mn_1 and Mn_2 atoms on two inequivalent lattice sites. An effective magnetic moment of $3.6 \mu_B$ was determined from the paramagnetic susceptibility²⁸. The occurrence of long-range antiferromagnetic order below the Néel temperature T_{N2} is accompanied by a distortion of the orthorhombic unit cell with lattice parameters $a_r \approx a_h$, $c_r \approx c_h$, and $b_r < \sqrt{3}a_h$ ^{28–30}. In the AF2 phase between T_{N2} and T_{N1} , the Mn_1 and one third of the Mn_2 atoms do not exhibit an ordered magnetic moment. The remaining Mn_2 atoms have magnetic moments $\mu \approx 1.5 \mu_B$ oriented parallel and antiparallel to the crystallographic b axis of the orthorhombic cell in a collinear fashion^{28,30}, see Fig. 1.

In the low-temperature antiferromagnetic AF1 phase below T_{N1} , the magnetic structure has monoclinic symmetry with atomic positions that can still be described with orthorhombic symmetry of the Cmmm space group without inversion symmetry^{28,29,31}. In this phase, the Mn_1 atoms acquire a moment presumably due to the expansion of the lattice along the crystallographic c axis and the accompanied increase of the Mn_1 - Mn_1 distance^{28–31}. The moments point into different directions forming a highly non-collinear antiferromagnetic structure, see Fig. 1. One third of the Mn_2 atoms still do not exhibit an ordered magnetic moment below T_{N1} . The non-collinearity is attributed to frustration^{29,30}. $T_{N2} = 100$ K and $T_{N1} = 62$ K have been also determined from susceptibility measurements, and indications of a third anomaly with hysteresis between 30 and 60 K have been found²⁸. In that work, a non-collinear phase has been suggested for $T < T_{N1}$ as well, however with a modified spin arrangement²⁸.

II. EXPERIMENTAL

A 160-nm thick Mn_5Si_3 film was prepared by magnetron sputtering from elemental targets on a sapphire substrate heated to 470 °C. A mechanical mask was used to obtain a Hall-bar configuration³². In addition, we dis-

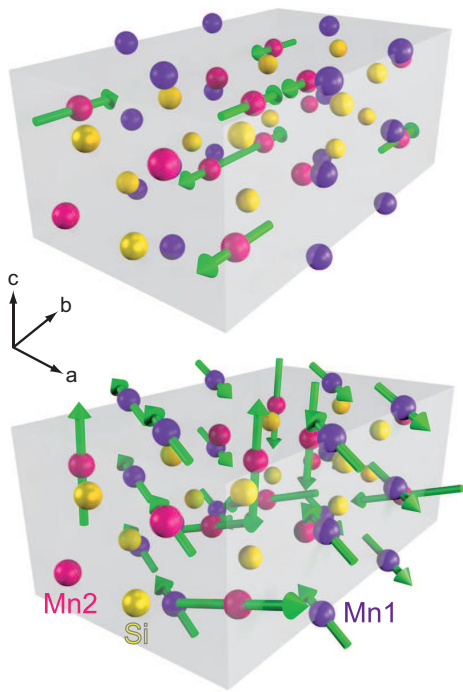


FIG. 1. Magnetic structure of Mn_5Si_3 (orthorhombic unit-cell) in the collinear AF2 phase (top) and in the low-temperature noncollinear AF1 phase (bottom) obtained from neutron scattering²⁹.

cuss data obtained on a 40-nm film which have been published earlier²⁰. The hexagonal structure of the polycrystalline film was confirmed by x-ray diffraction. Sputtered films prepared under the same conditions have a coarse-grained morphology with a grain size less than 100 nm³². The Mn_5Si_3 crystal was obtained by a combined Bridgman and flux-growth technique using a Mn-rich self flux and a low cooling rate of 1.2°C/h and was characterized by powder x-ray diffraction as well, again confirming the formation of the Mn_5Si_3 phase. A thin cuboid piece ($0.9 \times 3.9 \text{ mm}^2$) of 0.47 mm thickness with the crystallographic a_h and c_h axes aligned parallel to the long and short edge, respectively, and perpendicularly to the sample normal (z direction) was obtained after orientation by Laue diffraction. Resistivity and Hall-effect measurements were performed in a physical-property measurement system (PPMS) with the field oriented along the z direction perpendicular to the sample xy plane and with the current in plane. Hence, in the orthorhombic phase the magnetic field is along the b_r direction. Data were taken for both field directions and were symmetrized by $\rho_{xy}(H) = [\rho_{xy}(+H) - \rho_{xy}(-H)]/2$ for each field and by taking into account the direction of the measurement loop. Magnetization curves of the film and of the single crystal were acquired in a vibrating sample magnetometer up to 12 T and in a SQUID magnetometer up to 5 T with the field applied in the same orientation as for the Hall-effect measurements.

III. RESULTS

A. Thin films

The longitudinal resistivity ρ_{xx} [Fig. 2(a)] shows a behavior characteristic for an AFM with a linear temperature dependence in the paramagnetic regime and a 'hump-backed structure'³³ below the Néel temperature T_{N2} as observed earlier for polycrystals³⁴. From the derivative $d\rho/dT$ the transition temperatures $T_{N2} = 99 \text{ K}$ and $T_{N1} = 68 \text{ K}$ are obtained [Fig. 2(a), inset] in good agreement with values obtained for bulk polycrystals^{28–30}. T_{N2} is nearly independent of the magnetic field while the feature at T_{N1} diminishes with increasing field, see Fig. 2(a) inset.

The magnetization increases continuously with field without saturation and with a slope that strongly changes with temperature, see Fig. 2(b). The inset shows that $M(1 \text{ T})$ has a maximum close to T_{N1} . Finally, Fig. 2(c) shows the Hall resistivity ρ_{xy} for some selected temperatures in the noncollinear AF1 phase, at $T = 50 \text{ K}$ and 20 K well below T_{N1} , and at $T = 70 \text{ K}$ slightly above T_{N1} . While at the latter ρ_{xy} shows an almost linear behavior with magnetic field, the Hall resistivity in the noncollinear regime exhibits a kink at a field H^* indicated by an arrow.

For further analysis, we separated the contributions R_0B and ρ_{xy}^{AH} to the Hall resistivity (Eq. 1) using the whole set of magnetotransport data with focus on the high-field regime and assuming $\rho_{xy}^{AH} = S_H \rho_{xx}^2 M_z$ observed for ferromagnetic Mn_5Ge_3 (Ref. 35). A possible additional contribution varying only linearly with ρ_{xx} due to skew scattering does not change the obtained values R_0 and S_H due to the high resistivity of the film²⁰ and is therefore not further taken into account. The inset in Fig. 2(c) shows that $R_0 \approx 5 \times 10^{-10} \text{ m}^3/\text{As}$ and $S_H \approx 0$ above T_{N1} in the collinear antiferromagnetic and in the paramagnetic phases, i.e., the Hall effect is exclusively due to the ordinary contribution. Both Hall coefficients, R_0 and S_H strongly change below T_{N1} indicating a considerable change of the Fermi surface. In particular, S_H attains negative values of -0.02 V^{-1} at low temperatures. The solid lines in Fig. 2(c) show the field dependence of the Hall resistivity calculated from Eq. (1) with R_0 and S_H . The deviation between the data and the calculation (shaded area) is of the order of 20 nΩcm at $T = 20 \text{ K}$ and is attributed to a THE arising from the noncollinear magnetic structure in the AF1 phase for magnetic fields below H^* (Ref. 20).

B. Single crystal

The resistivity of the single crystal in the paramagnetic range above 100 K is reduced by only 35 % with respect to the polycrystalline film, see Fig. 3(a). Yet, the features of $\rho_{xx}(T)$ at the two transitions $T_{N2} = 100$

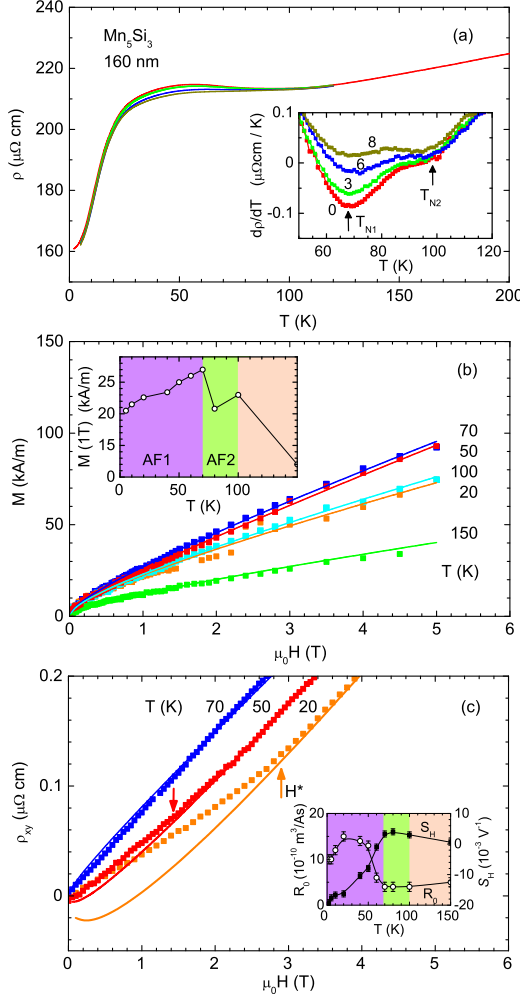


FIG. 2. Mn_5Si_3 film (160 nm): (a) Resistivity $\rho_{xx}(T)$, inset shows the derivative of ρ . (b) Magnetization $M(H)$ for various temperatures T . Inset shows M/H for $\mu_0 H = 1$ T. (c) Hall resistivity $\rho_{xy}(T)$ for various temperatures. Solid lines represent the calculated behavior of ρ_{xy} . Arrows indicate the critical field H^* below which the data deviate from the calculated Hall resistivity, Eq. 1. Inset shows the temperature dependence of the Hall coefficients R_0 and S_H .

K and $T_{N1} = 60$ K are much better resolved in the single crystal compared to the polycrystalline film. In the latter, averaging over all orientations in the electronic transport leads to a smearing of both transitions. Earlier resistivity measurements on Mn_5Si_3 single crystals also revealed two separate transitions³⁶. In a collinear AFM, the broad hump below the magnetic order-disorder Néel transition at T_{N2} is due to the formation of a magnetic superstructure larger than the crystal lattice and the new (smaller) Brillouin zone cuts the Fermi surface³³. The clear separation of the two transitions in the resistivity not only persists in magnetic field but, in fact, becomes even more pronounced. While T_{N2} of the paramagnet/collinear-antiferromagnetic transition does not change with field, the transition tem-

perature T_{N1} strongly decreases with increasing field. Neutron scattering and magnetic-susceptibility measurements on polycrystals already demonstrated that an applied magnetic field strongly reduces T_{N1} while T_{N2} remains unaffected^{28,31}. The field independence of T_{N2} is reminiscent of that of Mn_3Si (Ref. 37) and possibly due to the stability and strong anisotropy of Mn_2 moments. On the other hand, not only is T_{N1} suppressed markedly with field but, in addition, the resistivity at $T_{N1}(H)$ decreases strongly. At $T_{N1}(8\text{ T}) = 37\text{ K}$ the resistivity even drops below the low-temperature residual resistivity $\rho_{xx}(T \rightarrow 0)$ of the noncollinear phase. This confirms that the spin-dependent scattering is much stronger in the noncollinear phase than in the collinear phase with a bipartite magnetic structure.

The isothermal magnetization $M(H)$ plotted in Fig. 3(b) shows, for instance at $T = 50$ K, a sudden increase from a low-field magnetization, increasing linearly from $M(0) = 0$, to a much higher magnetization at a field H_c . Similar magnetization curves have been reported earlier^{36,38}. The jump at H_c was attributed to a metamagnetic transition from a low-field noncollinear phase to a high-field phase akin to the collinear phase observed in zero field above T_{N1} . The origin of a possible two-step transition at H_c has to be investigated further. This metamagnetic transition is not observed in the 160-nm film possibly due to structural disorder and strong demagnetization effects, see Fig. 2(a). At $T = 5$ K, $M(10\text{ T}) = 310\text{ kA/m}$ perfectly agrees with previously published data³⁶ and corresponds to a moment of $1.66\text{ } \mu_B/\text{Mn}_1$ or an average moment of $0.64\text{ } \mu_B/\text{Mn}$. We note that in the noncollinear phase at low fields the magnetization increases with increasing temperature while at fields above the metamagnetic transition the magnetization decreases with increasing temperature. The former resembles the thin-film behavior, cf. Fig. 2(b). A further detail is the weak hysteresis of $M(H)$ at ≈ 3 T well below the metamagnetic transition, exemplarily shown for $T = 50$ K in Fig. 3(b) inset.

The metamagnetic transition and the weak hysteresis are also observed in the magnetoresistivity [Fig. 3(c)] where the former leads to an almost 15 % reduction of the resistivity at 40 K as reported earlier³⁶. In the collinear phase at 75 K, only a weak magnetoresistivity is observed.

These two characteristics of the magnetic behavior of Mn_5Si_3 are most clearly observed in the Hall effect, exemplarily shown in Fig. 3(d) for three different temperatures. At 40 K, ρ_{xy} roughly linearly decreases to negative values with increasing field until, at $H^* \approx 2.5$ T, ρ_{xy} starts to increase with a sign change to positive values. Eventually, ρ_{xy} saturates and becomes independent of H until it sharply drops at a field corresponding to the metamagnetic transition at H_c . In the collinear phase at 75 K, ρ_{xy} shows an only weak increase compatible with $S_H = 0$ and $R_0 = 6 \times 10^{-10}\text{ m}^3/\text{As}$, similar to R_0 observed for the thin film above T_{N1} , cf. Fig. 2(c) inset. Moreover, for this orientation no hysteresis is observed for ρ_{xy} when the field sweeps through zero, see the raw

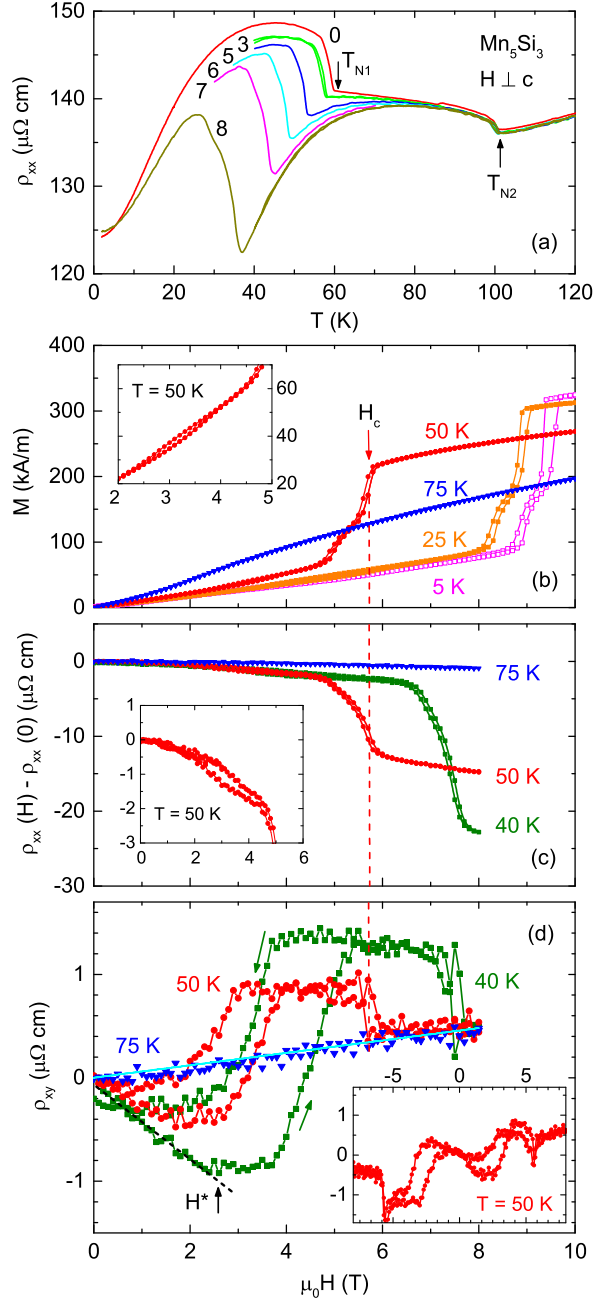


FIG. 3. Mn_5Si_3 single crystal with H applied along the z direction perpendicularly to the crystallographic c axis and current in the xy plane. (a) Resistivity $\rho_{xx}(T)$, numbers indicate the applied magnetic field in T. (b) Magnetization $M(H)$ in the collinear ($T = 75$ K) and noncollinear regime ($T = 50$ K, 25 K, and 5 K). Inset shows a small hysteresis observed at $T = 50$ K. (c) Magnetoresistivity. Inset shows a small hysteresis observed at $T = 50$ K. (d) Hall resistivity in the collinear ($T = 75$ K) and noncollinear regime ($T = 40$ and 50 K). Light blue line shows the ordinary Hall effect for $R_0 = 6 \times 10^{-10} \text{ m}^3 \text{ As}^{-1}$. Arrow and broken line indicate the critical field H_c of the metamagnetic transition for $T = 50$ K. Black dotted line indicates a linear decrease of ρ_{xy} up to a field H^* above which ρ_{xy} increases to positive values. The inset shows raw data for positive and negative magnetic field at $T = 50$ K.

data for $T = 50$ K in Fig. 3(d) (inset). Demagnetization effects have found to be negligible ($< 1\%$) when taking into account $N_z = 0.635$. Comparison of the AHE data confirms that at 40 and 50 K the (ordinary) Hall effect of the collinear phase at $T = 75$ K is recovered above H_c , suggesting that the field-induced phase below T_{N1} is similar to the zero-field collinear phase above T_{N1} . Between H^* and H_c an additional field-induced magnetic phase exists with an AHE $\rho_{xy}(3 \text{ T}) = 0.9 \mu\Omega\text{cm}$ that is nearly independent of field and magnetization. At $T = 25$ K an even larger $\rho_{xy}(5 \text{ T}) = 2 \mu\Omega\text{cm}$ corresponds to a Hall conductivity $\sigma_{xy} \approx \rho_{xy}/\rho_{xx}^2 = 102 \Omega^{-1}\text{cm}^{-1}$ despite a low magnetization of $M(5 \text{ T}) = 50 \text{ kA/m}$. Interestingly, ρ_{xy} also seems to be independent of the magnetoresistivity $\rho_{xx}(H)$ in this field range, cf. Fig. 3(c). When reducing the field to zero, the field-induced intermediate phase becomes energetically unstable against the non-collinear arrangement which then gives rise to a strong decrease of ρ_{xy} with a broad hysteresis of about 1 T.

IV. DISCUSSION

In the paramagnetic and in the collinear antiferromagnetic phases above $T_{N1} = 60$ K, the Hall effect of both Mn_5Si_3 films and single crystal is dominated by the ordinary contribution $\propto R_0 B$. At lower temperatures $T < T_{N1}$, the AHE of the single crystal shows a different behavior compared to the 160-nm film. For the single crystal, it is difficult to separate the contributions arising from the ordinary Hall effect and AHE and we discuss the results only qualitatively. Fig. 4 shows the characteristic fields H^* for two films and the single crystal following a similar behavior. Below H^* , the noncollinear spin arrangement facilitates a THE. However, the magnitude of the THE is much more pronounced in the single crystal compared to the polycrystalline films. The different sign of the small THE signal in the latter requires further investigations. The vanishing of the THE at H^* suggests the formation of two different field-induced phases, one between H^* , the critical field of the noncollinear state, and H_c , and one above the field H_c of the metamagnetic transition.

Below H^* , the Mn_1 ordered moments disturb Mn_2 moments leading to a tilting of all moments and to noncollinearity^{28,29,31}. The magnetic configuration changes by an applied magnetic field due to a magnetostructural change from monoclinic back to orthorhombic symmetry with a decrease of the Mn_1 - Mn_1 distance. This change causes a large inverse magnetocaloric effect²⁸. Neutron scattering suggests that in 1 T the sample is already in the AF2 phase at $T = 63$ K and likewise in 3.6 T at $T = 58$ K (Ref. 31). In 4 T, the orthorhombic phase established at 50 K remains down to the lowest measuring temperature of $T = 5$ K (Ref. 28). This interpretation of a stabilization of a collinear phase toward lower temperatures by a magnetic field is corroborated by the resistivity measurements [Fig. 3(a)]. However,

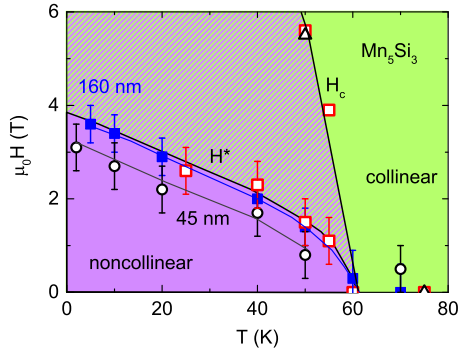


FIG. 4. Magnetic fields H^* and H_c determined from the Hall effect for the single crystal (increasing field-sweep) with H oriented perpendicularly to the crystallographic c axis (square symbols), and H^* of the 160-nm and 40-nm thick films²⁰. Triangles indicate H_c observed in $M(H)$.

the present results show that a collinear field-induced phase akin to the AF2 phase is only established above the metamagnetic transition H_c where the Hall resistivities above and below T_{N1} coincide. Between H^* and H_c , an additional field-induced phase generating a large positive AHE with hysteresis is inferred from our Hall-effect data. In this regime, ρ_{xy} changes sign from negative to positive and becomes independent of H and M . A possible scenario would be a weak ferromagnetic coupling of the Mn_1 moments still maintaining noncollinearity of the Mn_1 and Mn_2 moments.

V. CONCLUSION

Comparison of the AHE of antiferromagnetic Mn_5Si_3 films and a single crystal provides deeper insight into the magnetotransport properties compared to magnetoresistivity. Below a characteristic field H^* , the noncollinear behavior of different Mn_1 and Mn_2 moments is maintained in the film as well as in the bulk crystal. This suggests that the large AHE attributed to noncollinearity is generated on a length scale of a few nm and is a local property not relying on long-range magnetic order. The variation of the AHE is more pronounced in the single crystal, for which an additional metamagnetic transition is observed at higher fields $H_c(T) > H^*(T)$. The metamagnetic transition is not observed in the film possibly due to structural and magnetic disorder and/or strong demagnetizing fields. First-principle calculations of the band structure of the noncollinear phase are strongly needed to obtain the Berry-phase curvature for a quantitative discussion of the results.

ACKNOWLEDGMENTS

We thank P. Adelman for structural characterization of the single crystal and A. Granovsky and F. Weber for

helpful discussions.

- ¹A. H. MacDonald and M. Tsoi, Phil. Trans. Royal Soc. A **369**, 3098 (2011).
- ²R. Cheng, J. Xiao, Q. Niu, and A. Brataas, Phys. Rev. Lett. **113**, 057601 (2014).
- ³E. G. Tveten, A. Qaiumzadeh, O. A. Tretiakov, and A. Brataas, Phys. Rev. Lett. **110**, 127208 (2013).
- ⁴T. Jungwirth, X. Marti, P. Wadley, and J. Wunderlich, arXiv:1509.05296 [cond-mat] (2015).
- ⁵A. V. Kimel, B. A. Ivanov, R. V. Pisarev, P. A. Usachev, A. Kirilyuk, and T. Rasing, Nat. Phys. **5**, 727 (2009).
- ⁶N. Nagaosa, J. Sinova, S. Onoda, A. H. MacDonald, and N. P. Ong, Rev. Mod. Phys. **82**, 1539 (2010).
- ⁷T. Jungwirth, Q. Niu, and A. H. MacDonald, Phys. Rev. Lett. **88**, 207208 (2002).
- ⁸T. Miyasato, N. Abe, T. Fujii, A. Asamitsu, S. Onoda, Y. Onose, N. Nagaosa, and Y. Tokura, Phys. Rev. Lett. **99**, 086602 (2007).
- ⁹W. Jiang, X. Z. Zhou, and G. Williams, Phys. Rev. B **82**, 144424 (2010).
- ¹⁰E. A. Turov, V. G. Shavrov, and Y. P. Irkhin, Soviet Physics JETP **20**, 198 (1965).
- ¹¹Y. Taguchi, Y. Oohara, H. Yoshizawa, N. Nagaosa, and Y. Tokura, Science **291**, 2573 (2001).
- ¹²Y. Machida, S. Nakatsuji, S. Onoda, T. Tayama, and T. Sakakibara, Nature **463**, 210 (2010).
- ¹³B. G. Ueland, C. F. Mielea, Y. Kato, O. Ayala-Valenzuela, R. D. McDonald, R. Okazaki, P. H. Tobash, M. A. Torrez, F. Ronning, R. Movshovich, Z. Fisk, E. D. Bauer, I. Martin, and J. D. Thompson, Nat. Commun. **3**, 1067 (2012).
- ¹⁴N. Nagaosa and Y. Tokura, Nat. Nanotechn. **8**, 899 (2013).
- ¹⁵T. Schulz, R. Ritz, A. Bauer, M. Halder, M. Wagner, C. Franz, C. Pfeiderer, K. Everschor, M. Garst, and A. Rosch, Nat. Phys. **8**, 301 (2012).
- ¹⁶M. Hoffmann, J. Weischenberg, B. Dup, F. Freimuth, P. Ferriani, Y. Mokrousov, and S. Heinze, Phys. Rev. B **92**, 020401 (2015).
- ¹⁷H. Chen, Q. Niu, and A. MacDonald, Phys. Rev. Lett. **112**, 017205 (2014).
- ¹⁸J. Kübler and C. Felser, EPL **108**, 67001 (2014).
- ¹⁹O. Gomonay, Phys. Rev. B **91**, 144421 (2015).
- ²⁰C. Sürgers, G. Fischer, P. Winkel, and H. v. Löhneysen, Nat. Commun. **5**, 3400 (2014).
- ²¹A. Stroppa and M. Peressi, phys. stat. sol. (a) **204**, 4452 (2007).
- ²²C. Zeng, S. C. Erwin, L. C. Feldman, A. P. Li, R. Jin, Y. Song, J. R. Thompson, and H. H. Weitering, Appl. Phys. Lett. **83**, 5002 (2003).
- ²³C. Sürgers, K. Potzger, T. Strache, W. Müller, G. Fischer, N. Joshi, and H. v. Löhneysen, Appl. Phys. Lett. **93**, 062503 (2008).
- ²⁴I. Slipukhina, E. Arras, P. Mavropoulos, and P. Pochet, Appl. Phys. Lett. **94**, 192505 (2009).
- ²⁵V. L. Thanh, A. Spiesser, M.-T. Dau, S. F. Olive-Mendez, L. A. Michez, and M. Petit, Adv. Nat. Sci.: Nanosci. Nanotechnol. **4**, 043002 (2013).
- ²⁶I. A. Fischer, L.-T. Chang, C. Sürgers, E. Rolseth, S. Reiter, S. Stefanov, S. Chiussi, J. Tang, K. L. Wang, and J. Schulze, Appl. Phys. Lett. **105**, 222408 (2014).
- ²⁷J. B. Forsyth and P. J. Brown, J. Phys.: Condens. Matter **2**, 2713 (1990).
- ²⁸M. Gottschilch, O. Gourdon, J. Persson, C. de la Cruz, V. Petricek, and T. Brueckel, J. Mater. Chem. **22**, 15275 (2012).
- ²⁹P. J. Brown, J. B. Forsyth, V. Nunez, and F. Tasset, J. Phys.: Condens. Matter **4**, 10025 (1992).
- ³⁰P. J. Brown and J. B. Forsyth, J. Phys.: Condens. Matter **7**, 7619 (1995).
- ³¹M. R. Silva, P. J. Brown, and J. B. Forsyth, J. Phys.: Condens. Matter **14**, 8707 (2002).
- ³²B. Gopalakrishnan, C. Sürgers, R. Montbrun, A. Singh, M. Uhlarz, and H. v. Löhneysen, Phys. Rev. B **77**, 104414 (2008).
- ³³G. T. Meaden, Contemp. Phys. **12**, 313 (1971).

- ³⁴R. Haug, G. Kappel, and A. Jaégle, *phys. stat. sol. (a)* **55**, 285 (1979).
- ³⁵C. Zeng, Y. Yao, Q. Niu, and H. H. Weitering, *Phys. Rev. Lett.* **96**, 037204 (2006).
- ³⁶L. Vinokurova, V. Ivanov, E. Kulatov, and A. Vlasov, *Journ. Magn. Magn. Mater.* **90-91**, 121 (1990).
- ³⁷C. Pfleiderer, J. Bœuf, and H. v. Löhneysen, *Phys. Rev. B* **65**, 172404 (2002).
- ³⁸H. J. Al-Kanani and J. G. Booth, *Journ. Magn. Magn. Mater International Conference on Magnetism*, **140-144**